Characterization of Hurricane Eyes in RADARSAT-1 Images with Wavelet Analysis

Yong Du* and Paris W. Vachon♣
Natural Resources Canada
Canada Centre for Remote Sensing
588 Booth Street, Ottawa K1A 0Y7
Phone: 613 995-1575 (Vachon)
Fax: 613 947-1385
Email: Yong.Du / Paris.Vachon@ccrs.nrcan.gc.ca

Abstract

Striking examples of RADARSAT-1 synthetic aperture radar (SAR) images of hurricanes have been acquired over the past few years. The images show, with high resolution, the imprint of these storms on the ocean surface roughness, including structures associated with atmospheric processes such as boundary layer rolls, and details associated with the eye of the storm. In this paper, an image processing procedure for quantitatively characterizing SAR images of hurricane eyes (HEs) is described. The procedure uses the edge detection properties of wavelet analysis to estimate the scale and area of HEs. Procedures are also introduced to determine a reference elliptical aspect ratio (ratio of the major axis to the minor axis), the average radar cross-section, the position of the centre point, and an elliptical index. All indices are measured quantitatively and objectively. Based upon a visual examination, the estimated characteristics of HEs are reasonable. It is hoped that provision of a universal characterization procedure for SAR images of HEs will promote the use of RADARSAT-1 SAR images for the study of hurricane morphology.

Introduction

The calm eye of a hurricane shares many qualitative characteristics with other vortical systems in nature such as tornadoes, waterspouts, dust devils, and whirlpools. The characteristics of hurricane eyes (HEs) are strongly correlated with the hurricane's behaviour. Therefore, characterization of the HE allows us to explore the general mechanisms of hurricane evolution and to compare them with the properties of other vortical systems. Satellite images have been used for hurricane research for many years and offer the advantages of large area coverage and frequent repeat observation (e.g., Atlas and Black, 1994; Neumann, 1993; Gall et al., 1998; Hasler et al.,

*Under contract to CCRS from Noetix Research Inc., 265 Carling Ave., Suite 403, Ottawa, Ontario K1S 2E1 Canada.
♣ Corresponding author.

1998). Often, an HE may be observed in the infrared and visible channels of satellite imagery. However, atmospheric effects make it difficult for infrared and visible sensors to observe the fine details of the HE and eye wall on the ocean surface.

Synthetic aperture radar (SAR) images provide a high resolution, complementary view of hurricanes (e.g., Katsaros et al., 2000; Katsaros et al., 2002) through detection of their imprint on the ocean surface roughness distribution. Observation and modelling of the characteristics and properties of HEs, including their size and eye wall structure, have been important research topics (e.g., Brand, 1972; Willoughby et al., 1982; Merrill, 1984; Powell, 1990; Gray, 1991; Liu and Chan, 1999). We propose that RADARSAT-1 SAR images can be used to measure physical properties of HEs. To assess this opportunity, in this paper we consider and analyze RADARSAT-1 ScanSAR images of hurricanes that were acquired over the past few years. The objectives of the present paper are:

1. To suggest some quantitative characteristics of HEs;
2. To show that these characteristics are objective and universal; and
3. To develop practical methods of determining the characteristics of HEs from SAR images.

RADARSAT-1 Data

Since 1998, RADARSAT-1 SAR images of hurricanes have been acquired through a program known as Hurricane Watch, a collaboration between NRCan/CCRS (Natural Resources Canada, Canada Centre for Remote Sensing), CSA (Canadian Space Agency), and NOAA (National Oceanic and Atmospheric Administration) (see Vachon et al., 1998; 2001). CSA has taken a pro-active role in scheduling image acquisitions over hurricanes of interest around the world, usually in

ScanSAR wide mode (Luscombe et al., 1993). Many images that show all or a portion of an HE have been obtained and are available from the CCRS web site:

http://www.ccrs.nrcan.gc.ca/ccrs/rd/apps/marine/hurrican/overvu_e.html.

For the cases considered in this paper, the raw SAR signal data were processed to image products at CCRS on a workstation-based SAR processor. In each case, radiometrically calibrated, unsigned 16-bit integer standard format products with 50 m pixel spacing were produced. Subscenes of observed HEs were extracted (typically consisting of 2048 lines by 2048 pixels and covering a surface area of roughly 100 km by 100 km) and subsequently analyzed.

Quantitative Characteristics of HEs

Edge Detection

The lower wind speed associated with the HE results in a relatively smoother ocean surface. The reflected radar signal is very sensitive to changes in ocean surface roughness, and is relatively weak in the HE as compared to other areas in the storm. A key characteristic of the HE in a SAR images is its darker appearance. The darker appearance of an HE is different from the darker appearance of low wind shadow regions or oil spills, which are also seen in SAR images. For the HE, the dark region is surrounded by the eye wall, which contains the strongest wind speeds in the storm. There is a discontinuous wind speed boundary between the HE and eye wall. The darker appearance and discontinuous wind speed boundary are two common characteristics of well-defined HEs observed in SAR images.

The darker region of the HE is first roughly detected by using a threshold that is calculated as 90% of the mean radiometric value of the whole scene (Fig. 1). This area will vary depending on the relative area of the HE compared to the whole scene, but the centre of the HE is included. The

average values of x (the pixel number) and y (the line number) within the detected darker area are used as the initial HE centre location.

The maximum radiometric gradient points are then detected along polar directions from the initial HE centre location for all integer angles from 0° to 360° (Fig. 2). These maximum gradient points are shown in Fig. 3, which provides a discontinuous boundary. The average value of these points provides a threshold for determination of the HE extent. In this case, the extent of the HE is independent of the ratio of the mean radiometric value within the HE to that of the whole scene, and so, is objective (Fig. 4).

Although a logical approach, this edge detection procedure may not work satisfactorily in all cases. Because of noise (both speckle and thermal) in SAR images, individual darker samples within the scene but away from the HE could perturb the edge detection procedure. Therefore, a wavelet analysis is used to reject the higher frequency components caused by local noise. Experiments with wavelet multi-scale analysis have shown that good results are produced by using approximation images of level 5 with a ***db4*** wavelet basis (see Du et al., 2002; 2003). The pixel spacing of a RADARSAT-1 ScanSAR wide mode image is 50 m, so the level 5 approximation corresponds to a spatial frequency of 50 m $\times 2^5 = 1.6$ km. At this scale, HEs are detected with a low frequency wave around their edge.

The SAR images were decomposed using a wavelet multi-scale analysis prior to edge detection. The level 5 approximation was then reconstructed and the method described previously (Figs. 1 through 4) was used to detect the edge of the HE. We have not carried out a detailed comparison of the two approaches, but we favour using the level 5 image since it rejects noise elements that are not related to HE properties. The detected edge is generically referred to as the eye wall boundary.

Centre Location

Following edge detection, the spatial extent of the HE may be determined objectively. Since the HE is generally of irregular shape, we have used the average value of the grid values (X_i, Y_i) within the HE to define the centre point. That is:

$$X_c = \bar{X} = \frac{1}{n}\sum_{i=1}^{n} X_i \tag{1}$$

$$Y_c = \bar{Y} = \frac{1}{n}\sum_{i=1}^{n} Y_i \tag{2}$$

where X_c and Y_c are the centre position (indicated by * in Fig. 4), X_i and Y_i are the grid points around the detected edge, and n is the total number of points along the detected edge.

It should be pointed out that, although the calculation is not difficult, the centre point location is important for description of the HE. Because estimation of the centre point is objective and consistent for all HEs, in principle, the movement of an HE can be calculated and compared objectively from image to image.

Size and Reference Ellipse

When the spatial extent of the HE is determined, its area can be calculated trivially as the number of pixels within the spatial extent of the HE multiplied by the pixel size of the SAR image. That is:

$$A = N\ \delta x^2 \tag{3}$$

where A is the area and N is the number of pixels within the spatial extent of the HE.

It is apparent that, although irregular, the shape of most HEs is close to elliptical. By using the largest distance (L_d) between two points on the detected edge of the HE, the major axis (a) of the reference ellipse is estimated as $a = L_d / 2$. Then, by setting $A = \pi ab$, the minor axis b may be calculated trivially. Since the centre point of the reference ellipse coincides with that of the HE (Fig. 5), the aspect ratio of the reference ellipse ($R_a = a / b$, the ratio of the major axis to the minor axis) can be used as a rough descriptor of the HE's shape.

Elliptical Index

To determine the orientation of the major axis of the reference ellipse, the reference ellipse may be rotated around the common central point and the overlapping areas between the HE and the reference ellipse may be calculated. We made this calculation at every integer degree from 0° to 90° (Fig. 6). The angle with the largest overlap area is taken as the orientation of the major axis (Fig. 7). The ratio of the largest overlap area to the area of the HE is referred to as the Elliptical Index (*EI*), which represents how close the shape of the HE is to an ellipse. As *EI* approaches 1, the HE is closer to an ellipse. *EI* might provide clues as to the energy exchange crossing the edge of the HE. If $EI \to 1$, the boundary of the HE is rather smooth. If $EI << 1$, the boundary of the HE is rather rough.

Variability Along the HE Edge

The distance between the central point of the HE and the measured edge of the eye wall was estimated and plotted in 1-dimension to show the relative variation of the estimated eye wall boundary. This distance set was then filtered with a wavelet transform. After removing the low frequency component, the variability along the HE edge was analyzed and the mean wavelength, mean amplitude, maximum wavelength, and maximum amplitude were estimated (Fig. 8). Within

the HE itself, we can density slice or contour the observed intensity to better reveal SAR-observed structures within the HE (Fig. 9).

Summary

Quantitative characteristics of HEs as observed in RADARSAT-1 ScanSAR images have been suggested and estimated using wavelet-based image processing technique. Estimated parameters include the HE boundary (nominally the eye wall location), the surface area, the properties of a reference ellipse (a and b), the optimal orientation of the reference ellipse, the elliptical index (*EI*), and the variability of the eye wall boundary around the HE. The proposed procedure is objective, so it could be used to characterize the SAR image of any well defined HE. Fig. 10 provides a flowchart for this image processing procedure. Of course, other parameters could also be derived from these quantitative characteristics, such as maximum, minimum, and average radar cross-section within HE, as well as measurement of secondary brightness structures within the HE.

Measurements and Discussion

The proposed procedure was applied to eight RADARSAT-1 ScanSAR images with well defined HEs (Figs. 11). The pixel size was first reduced from 50 *m* by 50 *m* to 100 *m* by 100 *m* by block averaging. The resulting characterizations are summarized in Table 1. The average major axis of the eight HEs is 26.4 km, with a maximum of 52.8 km and minimum of 13.1 km. The average minor axis is 15.7 km, with a maximum of 38.8 km and a minimum 7.3 km. These numbers provide an accurate description of the shapes of the observed HEs. Therefore, *EI* could be used as an index to describe the ellipse and generically define each HE. On the other hand, the ratio between a and b ranges from 1.4 to 2.1 for well-defined HEs. This parameter provides insight as to whether or not the HE is close to round. The average area of the observed HEs is roughly 1676 km^2.

Conclusions

In this study, a procedure for the characterization of HEs observed in RADARSAT-1 ScanSAR images of the ocean has been developed. The proposed indices describe the HEs quantitatively and objectively. The determined boundary of the HEs allows discussion of the properties both inside and outside of the HE. Since the properties of the high wind area (outside of the HE) and the low wind area (inside of the HE) are significantly different, it is desirable that these two regions be analyzed separately. Furthermore, characterization of HEs by using an objective method can promote research on HEs by providing standard statistical information.

Further research will combine the proposed characterization of the HE with other SAR-derived properties (e.g., wind speed field, internal structure of the HE, etc.) to explore the form, development, and evolution of the hurricane.

Acknowledgements

We thank Patricia Voumard and Greta Burger (CSA / Satellite Operations) for their interest in Hurricane Watch and for their significant planning efforts that ensured the acquisition of the images discussed in this paper. We also thank Gunar Fedosejevs (CCRS) for his helpful suggestions and comments on the manuscript.

References

Atlas, D., and Black, P.G. 1994. The Evolution of Convective Storms from Their Footprints on the Sea as Viewed by Synthetic Aperture Radar from Space. *Bulletin of the American Meteorological Society*, Vol. 75, pp. 1183–1190.

Brand, S. 1972. Very large and very small typhoons of the western North Pacific Ocean. *Journal of the Meteorological Society of Japan*, Vol. 57, pp. 332-341.

Du, Y., Vachon, P.W., and Wolfe, J. 2002. Wind Direction Estimation from SAR Images of the Ocean Using Wavelet Analysis. *Canadian Journal of Remote Sensing*, Vol. 28, No. 3, pp. 498-509.

Du, Y., Vachon, P.W., and van der Sanden, J.J. 2003. Satellite Image Fusion with Multi-scale Wavelet Analysis for Marine Applications: Preserving Spatial Information and Minimizing Artifacts (PSIMA). In press, *Canadian Journal of Remote Sensing*.

Gall, R., Tuttle, J., and Hildebrand, P. 1998. Small-Scale Spiral Bands Observed in Hurricanes Andrew, Hugo, and Erin. *Monthly Weather Review*, Vol. 126, pp. 1749–1766.

Gray, W.M. 1991. Comments on "Gradient balance in tropical cyclones". *Journal of Atmospheric Science*, Vol 48, pp.1201-1208.

Hasler, A.F., Palaniappan, K., Kambhammetu, C., Black, P., Uhlhorn, E., and Chesters, D. 1998. High- Resolution Wind Fields Within the Inner Core and Eye of a Mature Tropical Cyclone from GOES in 1-min Images. *Bulletin of the American Meteorological Society*, Vol. 79, pp. 2483–2496.

Katsaros, K., Vachon, P., Black, P., Dodge, P., and Uhlhorn, E. 2000. Wind fields from SAR: Could they improve our understanding of storm dynamics? *Johns Hopkins APL Technical Digest*, Vol. 21, No. 1, pp. 86-93.

Katsaros, K.B., Vachon, P.W., Liu, W.T., and Black, P.G. 2002. Microwave remote sensing of Tropical Cyclones from Space. *Journal of Oceanography*, Vol. 58, pp. 137-151.

Liu, K.S. and Chan, J.C.L. 1999. Size of tropical cyclones as inferred from ERS-1 and ERS-2 data. *Monthly Weather Review*, Vol. 127, pp. 2992–3001.

Luscombe, A.P., Ferguson, I., Sheperd, H., Zimcik, D.G., and Navaine, P. 1993, The RADARSAT Synthetic Aperture Radar Development, *Canadian Journal of Remote Sensing*, Vol. 19, No. 4, pp. 298-310.

Merrill, R.T. 1984. A comparison of large and small tropical cyclones. *Monthly Weather Review*, Vol. 112, pp. 1408-1418.

Neumann, C.J. 1993. Global Overview. WMO/TC-No. 560, Report No.TCP-31, World Meteorological Organisation, Geneva.

Powell, M.D. 1990. Boundary Layer Structure and Dynamics in Outer Hurricane Rain Bands. Part I: Mesoscale Rainfall and Kinematic Structure. *Monthly Weather Review*, Vol. 118, pp. 891–917.

Vachon, P.W., Katsaros, K., Black, P., and Dodge, P. 1999. RADARSAT Synthetic Aperture Radar Measurements of Some 1998 Hurricanes. Proc. IEEE 1999 International Geoscience and Remote Sensing Symposium (IGARSS'99), 28 June to 3 July 1999, Hamburg, Germany, pp. 1631-1633.

Vachon, P.W., Black, P.G., Dodge, P., Katsaros, K.B., Clemente-Colón, P., Pichel, W.G., MacDonell, K. 2001. RADARSAT-1 Hurricane Watch. Proc. IEEE 2001 International Geoscience and Remote Sensing Symposium (IGARSS 2001), 9 to 13 July 2001, Sidney, Australia, on CD-ROM, 3p.

Willoughby, H.E., Clos, J.A., and Shoreibah, M.G. 1982. Concentric Eye Walls, Secondary Wind Maxima, and the Evolution of the Hurricane Vortex. *Journal of Atmospheric Science*, Vol. 39, pp. 395–411.

LIST OF TABLES:

LIST OF FIGURES:

Name	Date&Time	Latitude (N)	Longtitude (W)	Presure (mb)	Wind Speed (kt)	Stage	Life time	Size (km)	Maturity		
Danielle	Aug.31,98 10:48	29.1	74.1	977.0	88.0	H2 (+)	24 Aug.-3 Sept.	102.4X102.4	well defined		
Dennis	Aug.27,99 23:15	26.1	76.1	983.0	69.0	H1 (+)	24 Aug.-7 Sept	102.4X102.4	well defined		
Floyd	Sept.15,99 11:10	29.2	78.8	942.0	102.0	H3 (-)	7-17 Sept.	102.4X102.4	well defined		
Florence	Sept.13,00 10:53	29.7	71.4	997.0	49.0	TS(+)	10-17 Sept.	102.4X102.4	well defined		
Erin	Sept.11,01 22:19	38.0	64.5	976.0	80.0	H1 (=)	1-15 Sept.	102.4X102.4	well defined		
Erin	Sept.13,01 10:04	38.6	60.7	982.0	70.0	H1 (=)	1-15 Sept.	102.4X102.4	well defined		
Humberto	Sept.26,01 21:42	42.1	55.2	985.0	72.0	H1 (-)	21-27 Sept.	102.4X102.4	well defined		
Olga	Nov.28,01 09:49	32.5	56.7	976.0	75.0	H1 (=)	24 Nov.- 4 Dec.	102.4X102.4	well defined		
Average		33.2	67.2	977.3	75.6						

Name	a (km)	b (km)	a/b	Area (km^2)	Slope (˚)	*EI*	Max Amplitude	Mean Amplitude	STD	Max Wave-length	Mean Wave-length
Danielle	19.0	11.9	1.6	709.0	27.0	1.0	1.0	0.5	4.4	23.1	14.7
Dennis	32.9	15.5	2.1	1607.0	18.0	0.9	2.5	1.0	9.9	39.4	19.8
Floyd	35.3	23.2	1.5	2568.2	45.0	0.9	3.5	1.6	12.4	50.8	35.5
Florence	21.4	10.4	2.1	696.0	20.0	0.9	1.5	0.7	6.0	29.0	16.8
Erin	16.2	7.7	2.1	392.0	18.0	0.8	2.4	1.2	9.2	29.0	19.9
Erin	52.8	38.8	1.4	6442.0	19.0	0.9	4.3	1.4	13.9	90.0	42.4
Humberto	13.1	7.3	1.8	300.4	21.0	0.9	1.4	0.6	4.5	16.9	9.0
Olga	20.2	10.9	1.9	693.0	18.0	0.9	1.7	0.7	6.3	32.9	19.3
Average	26.4	15.7	1.8	1676.0	23.3	0.9	2.3	1.0	8.3	38.9	22.2

Table 1

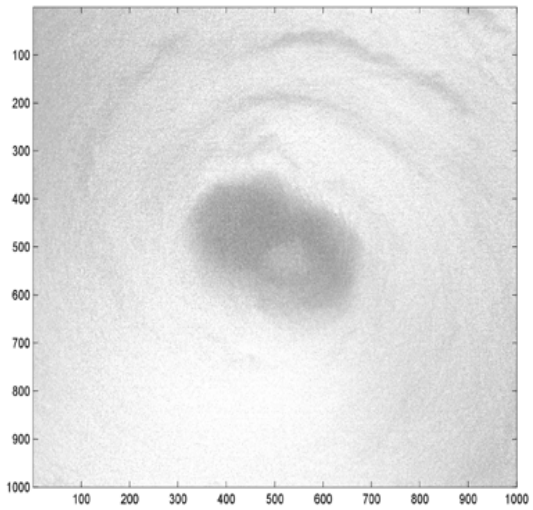

Fig. 1a

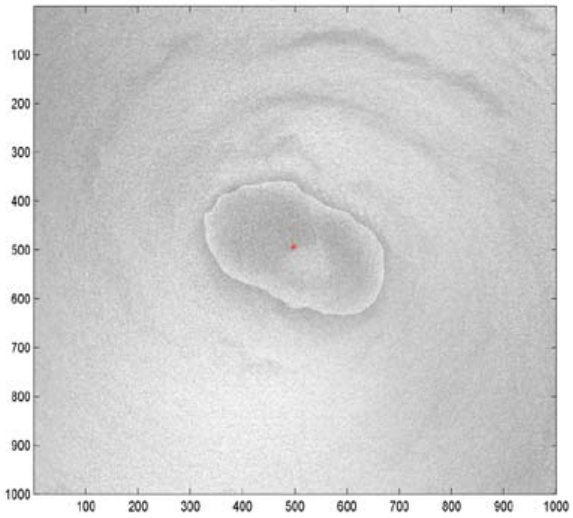

Fig.1b

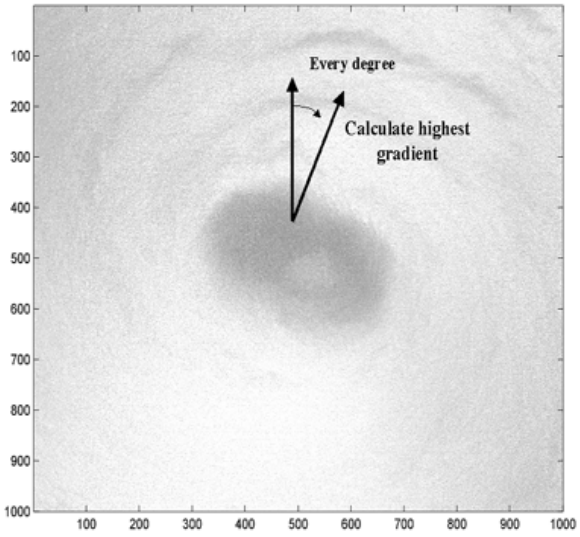

Fig. 2

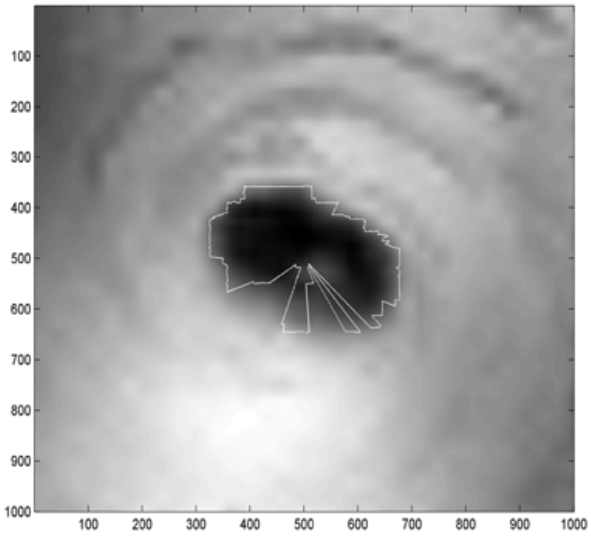

Fig.3

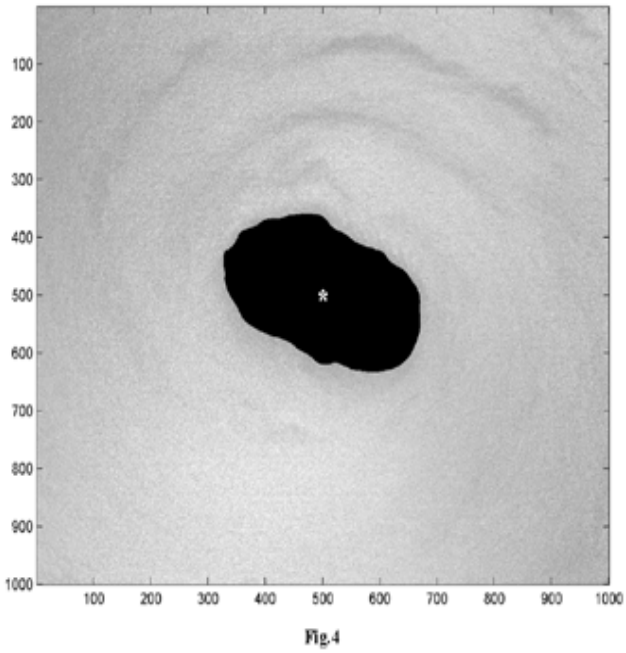

Fig.4

Fig. 4

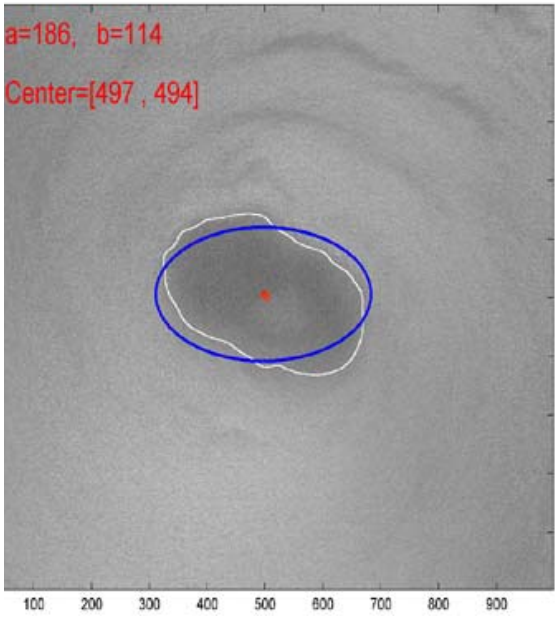

Fig.5

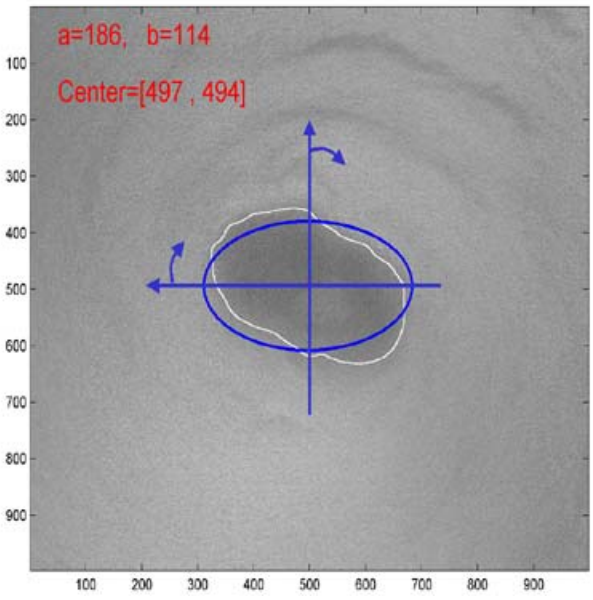

Fig. 6

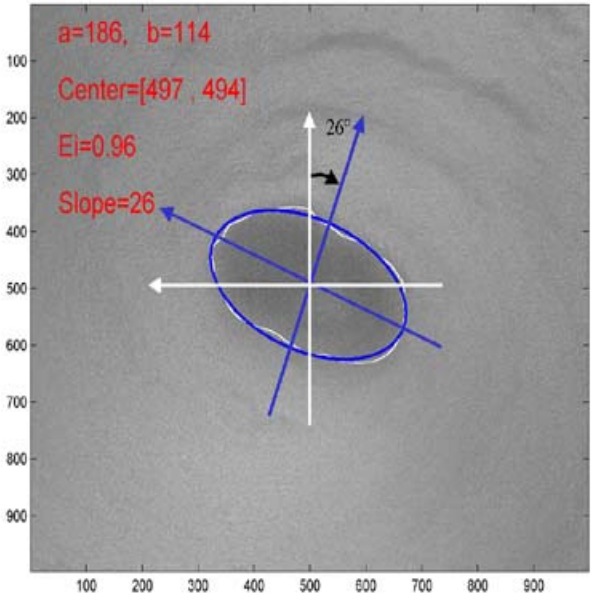

Fig.7

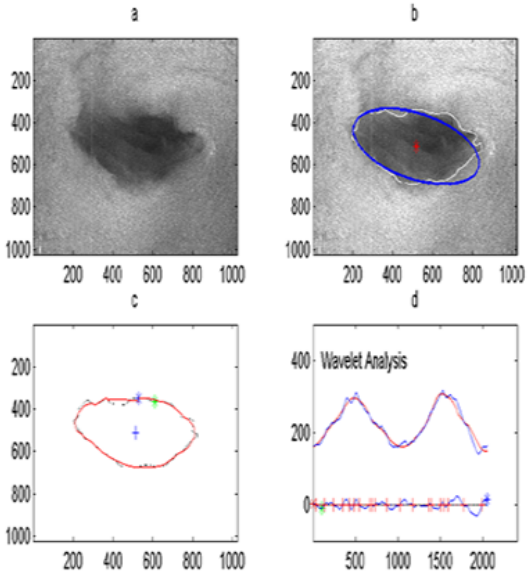

Name: Dennis, Time: Aug. 27, 1999 23:15(UTC), Size: 102.4X102.4(km2)

a=32.9(km), b=15.5(km), a/b=2.12

Area=1607(km2), Slope=18(degree), Ei=0.89

Max Amplitude=2.5(km), Mean Amplitude=1(km) Std=9.91

Max WaveLength=39.4(km), Mean WaveLength=19.8(km)

Fig. 8

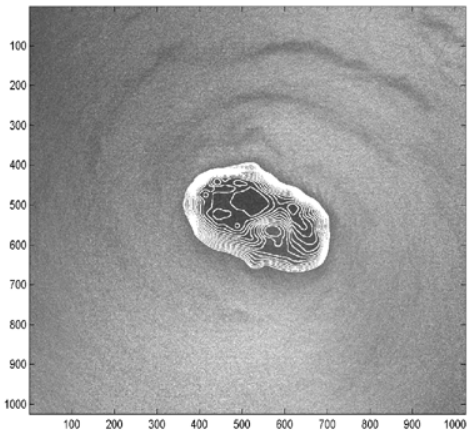

Fig. 9

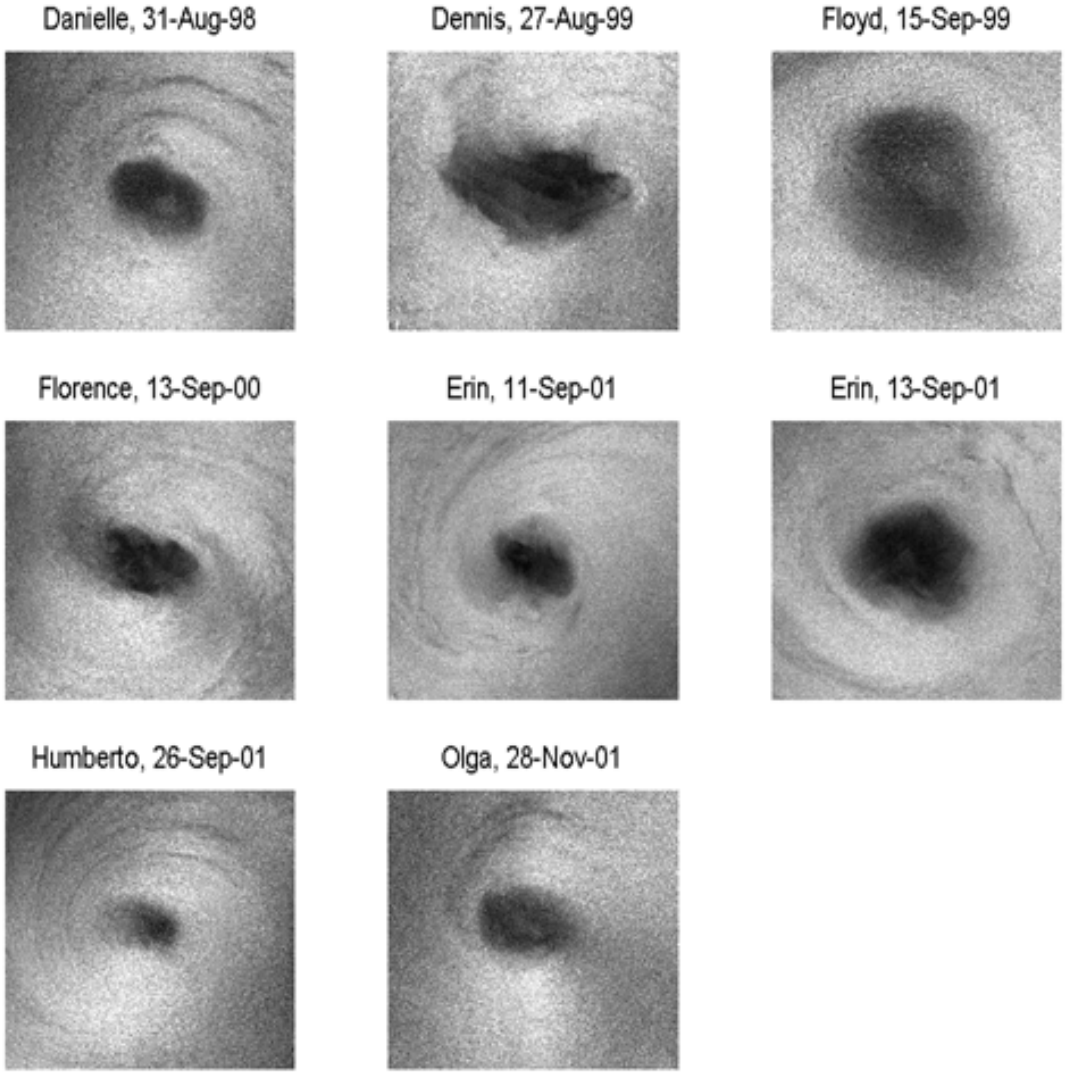
Danielle, 31-Aug-98
Dennis, 27-Aug-99
Floyd, 15-Sep-99
Florence, 13-Sep-00
Erin, 11-Sep-01
Erin, 13-Sep-01
Humberto, 26-Sep-01
Olga, 28-Nov-01

Fig. 11

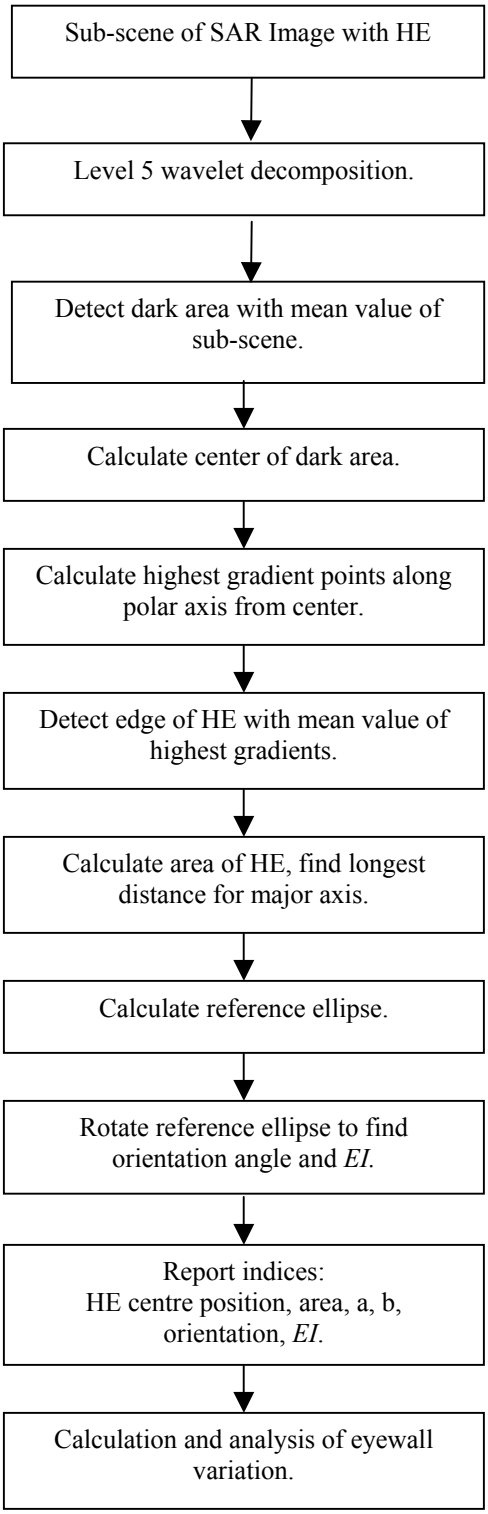
Sub-scene of SAR Image with HE
Level 5 wavelet decomposition.
Detect dark area with mean value of sub-scene.
Calculate center of dark area.
Calculate highest gradient points along polar axis from center.
Detect edge of HE with mean value of highest gradients.
Calculate area of HE, find longest distance for major axis.
Calculate reference ellipse.
Rotate reference ellipse to find orientation angle and *EI*.
Report indices:
HE centre position, area, a, b, orientation, *EI*.
Calculation and analysis of eyewall variation.

Fig. 10